ELSEVIER

Polymer 41 (2000) 7559–7573

polymer

Toughening of a polysilsesquioxane network by homogeneous incorporation of polydimethylsiloxane segments

B. Zhu[a,*], D.E. Katsoulis[a], J.R. Keryk[a], F.J. McGarry[b]

[a]*Central R&D, Dow Corning Corporation, Mail Stop #500, 3901 S. Saginaw Road, Midland, MI 48686, USA*
[b]*Department of Materials Science and Engineering, Massachusetts Institute of Technology, Cambridge, MA 02139, USA*

Received 14 April 1999; received in revised form 3 August 1999; accepted 22 December 1999

Abstract

Methods were developed to characterize the fracture behavior of a condensation cure polysilsesquioxane network, and to toughen the network with homogeneously incorporated polydimethylsiloxane (PDMS) segments. Hydroxyl terminated PDMS short chains were end-capped with tetraethoxy silane and the end-capped segments were coupled with the oligomeric silsesquioxane bearing silanol ends. The end-capping and the coupling reactions were investigated by FT-IR, ^{29}Si and ^{1}H NMR, and GPC. The complete end-capping of the PDMS chains was achieved with minimum self-condensation and cyclization, and a complete coupling of the functionalized PDMS with the oligomeric silsesquioxane was achieved with no self-condensation of the PDMS chains. To toughen the network such a coupling reaction was necessary, otherwise PDMS chains formed a separate phase which was ineffective. Short PDMS chains and silsesquioxane oligomers were incompatible and a ternary phase diagram with toluene as the third component was constructed to define a concentration window for the coupling reaction. When homogeneously reacted into the resin network, all the PDMS chains of degrees of polymerization (DP) between 8 and 55 increased the fracture toughness, and within this range the longer chains were more effective. Ten parts of PDMS of DP 55 increased the K_{Ic} from 0.253 to 0.456 MPa $m^{1/2}$, and G_{Ic} from 34.1 to 151.11 J/m^2. TGA showed the thermal stability of the network was retained after PDMS toughening. Enhanced inelastic deformation was responsible for the increased fracture toughness. Upon re-initiation of a crack, the toughened network developed a plastic zone the size of which was consistent with the calculated zone from Irwin's model, while no evidence of such yielding was seen for the untoughened network.

Keywords: Polysilsesquioxane; Fracture toughness; Toughening

1. Introduction

Many polymers are brittle or notch sensitive under certain stress conditions and extensive research has been devoted to improving such properties [1–14]. In addition to modification of the molecular architecture of a polymer at the synthesis stage, alteration of the morphology by controlled processing or by incorporating second phase materials can have a profound impact on polymer fracture toughness [15–18]. Rubber particles are the most often used second phase materials; in many cases they result in a multi fold increase in fracture toughness [19–25]. A well-known example is toughened epoxy resins [26]. A great variety of rubber and resin systems have been studied and the toughening mechanisms have been investigated. It is believed that the rubbery particles relieve the triaxiality of stress ahead of the crack tip and facilitate yielding of the matrix [27–29]. The stress state can be altered by the mismatch of coefficients of thermal expansion of the matrix and dispersed phases [28], by the stress concentration induced by the more compliant particles when the material is under tension [29], and by cavitation of the particles [30–32]. Usually the size of the rubber particles, the interfacial adhesion, and the rubber cohesive strength are important parameters for optimal toughening.

Highly crosslinked thermosets are difficult to toughen by rubbery inclusions, because little crack tip plastic deformation occurs in such materials. Several studies have demonstrated that the toughenability of a network depends on the matrix capability to undergo plastic deformation [33–35]. With glassy polysilsesquioxane networks, the matrix properties have to be modified before the incorporation of a second rubbery phase.

Polysilsesquioxanes have attracted much attention. They can be most broadly described by an empirical formula $(RSiO_{3/2})_n$, where R is an alkyl group, hydrogen, or a combination of different alkyl groups. Although they possess

* Corresponding author. Tel.: + 1-517-496-3059.
E-mail address: bizhong.zhu@dowcorning.com (B. Zhu).

0032-3861/00/$ - see front matter
PII: S0032-3861(00)00027-6

Table 1
Materials used to synthesize functionalized PDMS

Name	Supplier	Comment
Tetraethyl orthosilicate	Pfaltz & Bauer, Inc.	99% pure
Potassium acetate	Aldrich	99+% pure
Phenyl trimethoxy silane	United Chemical, Technologies, Inc.	
FA fluid	Gelest, Inc.	Silanol terminated PDMS, degree of polymerization (DP): 6.
FB fluid	Dow Corning Corp.	Silanol terminated PDMS, DP 15.
FC fluid	Dow Corning Corp.	Silanol terminated PDMS, DP 55.
4-3136 Binder resin	Dow Corning Corp.	Condensation cure silicone resin with silanol ends.
Titanium tetrabutoxide	Aldrich	99% pure

extraordinary heat and fire resistance, their brittleness has prevented any utilization of their potential. To counter this problem, in commercially available products a small amount of linear siloxane blocks is copolymerized into the structure, with a limited degree of success. The rubber particle approach has not been successfully implemented in these networks. Polysilsesquioxanes have been traditionally used for non-load bearing applications such as fiber reinforced electric panels [36–38], insulation for electric motors, coatings [39–47], adhesives and electronics packaging [48–52], and resist material for microlithography [53,54]. Even for these applications facile crack initiation and propagation are a major problem [55]. The use of them for structural purpose is not practical without significant toughening. Recently polysilsequioxanes are being used as interlayer dielectric insulators because of their low dielectric constant. But their brittle nature often prevents the formation of thick films without cracks, and this complicates their processing. Improved toughness, with their thermal, fire, and electrical properties maintained, is highly desirable [55].

In this paper, a scheme to modify the mechanical properties by homogeneously reacting functionalized polydimethylsiloxane (PDMS) segments into a predominantly polysilsesquioxane network is presented. In a later report we will show that after these properties are improved, rubber particles are effective toughening for polysilsesquioxane networks [55].

2. Experimental

2.1. Materials

The chemicals listed in Table 1 are used as received without further purification. The 4-3136 binder resin, commercially available from Dow Corning Corporation, was produced by co-hydrolyzing a mixture of 85% (mol) trichlorosilanes and 15% (mol) dichlorosilanes (specified in Table 5) in toluene and an excess amount of water, washing the toluene phase with deionized water to remove hydrogen chloride, and condensing the toluene solution under heat. The resin was flaked to produce a soluble solid that had a Mn of 1410 and a M_w/M_n value of 1.805, as determined by GPC using polystyrene standards. The terminating groups of the resin were mostly silanol and some isopropoxy groups. In this paper the term "resin" is used for such a prepolymer before cure, while the cured resin is referred to as a "network".

Table 2
Functional PDMS

Name	Targeted DP	Actual DP	Type of end group
FAE	8	8.05	Triethoxy siloxy
FBE	16	16.5	Triethoxy siloxy
FCE	57	58.9	Triethoxy siloxy
FBM	16	16.7	Phenyl dimethoxy siloxy

2.2. Preparation of triethoxy and dimethoxy siloxy terminated polydimethylsiloxane

PDMS of degree of polymerization (DP) 14, triethoxy siloxyl terminated. A 500 ml three necked, round bottomed Pyrex glass flask was equipped with a stirrer, a condenser, a Dean Stark trap under the condenser, and connected to a vacuum system through the condenser. 100 g of FB fluid (a silanol terminated PDMS of DP 14, ~0.19 mol OH) and 190 g of tetraethyl orthosilicate (TEOS, 0.91 mol) were mixed in the flask and 0.29 g of dry potassium acetate was added. The mixture was heated slowly under nitrogen while being stirred. When the temperature reached 115°C volatile substances were distilled out, condensed, and collected in the trap. The temperature was maintained at 120–146°C. From time to time samples were taken from the flask and checked by FT-IR. The completion of the reaction was indicated by the disappearance of the broad peak centered at 3312 cm^{-1} for the terminal silanol. After the completion of the reaction the excess TEOS was removed by vacuum distillation. Finally potassium acetate was removed by filtration and a clean, transparent, colorless liquid was obtained.

PDMS of other DP or termination. Essentially the same process was used for PDMS short chains of different degrees of polymerization. The molar ratio of TEOS to PDMS was maintained at ten. The other termination was phenyl dimethoxy siloxy, and it was obtained by phenyl trimethoxy silane end capping of hydroxyl terminated PDMS. The same

Table 3
^{29}Si chemical shifts and their assignments

δ (ppm)	Assignment	Comments
0	Me_4Si	Reference
−19.3	$(Me_2SiO)_4$ (D_4)	Peak linewidth <0.5 ppm
−20.2 to −22.8	$(Me_2SiO)_n$ (linear or cyclics of $n > 5$) (D)	Narrow, overlapping peaks
−87.6 to −88.8	$(EtO)_3SiO_{1/2}$	Narrow peaks
−94.7 to −95.5	$O_{1/2}(EtO)_2SiO_{1/2}$	Due to PDMS self condensation

process was also used except for the molar ratio between the end capper and the PDMS. A ratio of twenty was maintained to overcome the tendency of methoxy to self condense due to its higher moisture sensitivity.

The designations of the prepared functional PDMS, their DP which was determined by ^{29}Si NMR, and the functionalities are listed in Table 2.

2.3. Construction of room temperature ternary phase diagrams

Visible turbidity of the mixture of 4-3136 resin/toluene/functionalized PDMS was used as the criterion of phase separation and the homogeneous/heterogeneous boundary was determined by a turbidity titration. For all PDMS oligomers, the turbidity transition was sharp enough for unaided eyes to detect accurately. However, it was noticed that the lower the degree of polymerization of PDMS, the less obvious the turbidity transition and the harder it was to detect an accurate transition. To construct a phase diagram, two series of solutions were prepared. One series was the 4-3136 resin solution in toluene with concentrations from 5 to 80 wt%, at a 5 wt% interval. Another series was PDMS solutions in toluene of the same concentrations. Two steps were needed to complete the construction of a room temperature ternary phase diagram. In the first step, PDMS was added to a 4-3136 resin toluene solution of known concentration so that the composition moved along a straight line toward the pure PDMS corner until the turbidity transition was encountered. Starting with the resin solutions of different concentrations, points along the homogeneous/heterogeneous boundary could be determined and a half of the curve was obtained. The second step was to obtain the other half of the curve. For this the PDMS solutions in toluene were used. Into these solutions a 60 wt% 4-3136 toluene solution was added gradually so that the composition moved along a curved trajectory on the phase diagram towards the pure resin corner until the homogeneous/heterogeneous boundary was encountered. In the same way as in step 1, points on the boundary curve were determined and the other half of the boundary was obtained. This method assumed that either the phase diagram was rather simple, or in the case of a complex phase diagram the part of interest would be obtained.

2.4. Coupling reaction of the functionalized PDMS with the resin

The 4-3136 resin and the PDMS segments are generally not miscible. When they were co-cured simply by mixing and curing at an elevated temperature with 0.1–0.4 wt% Dow Corning Catalyst Y-177®, a phase separated network was obtained. The Dow Corning Catalyst Y-177® is a mixture of 7% zinc octoate, 3% choline 2-ethylhexanoate in 47% *n*-butyl alcohol, 30% toluene and 12% Stoddart solvent. When the resin and the PDMS segments were pre-coupled and then cured, a homogeneous network was obtained without phase separation. To pre-couple the resin and the PDMS, they were dissolved in toluene and heated at 95°C for 28 h in the presence of a catalyst, 0.1–0.4 wt% titanium tetrabutoxide. Depending on the chain length of the PDMS, the amount of toluene added to compatiblize the resin and the PDMS was determined by the phase diagram.

2.5. Casting techniques

There are no reports of reliable measurement of the mechanical properties and fracture toughness of condensation cured polysilsesquioxane resins in the literature, primarily because of the difficulty of obtaining thick, fully cured, void free castings of these resins. The evolution of volatiles during cure makes it very difficult to avoid bubbles in the cured resin. However, the use of a relatively thick sample is necessary in a fracture toughness test to ensure a plane strain condition, since indentation methods, which involve less demanding sample preparation, are unreliable for materials with substantial plastic deformation [56].

To make a void free condensation cured cast plate, it was necessary to prevent the accumulation of water vapor in the casting during cure. To eliminate voids the condensation reaction rate was lowered by using lower levels of catalyst and a slow temperature ramping process. The diffusion of water was accelerated by using a mold shown in Fig. 1. The top of the mold was open to air to facilitate the removal of water. Two processes were used. In the melt process the solid resin was melted at 90–100°C and mixed with other ingredients, typically 0.05% Dow Corning Catalyst Y-177® and modifying agents if needed. The molten mixture was poured into the mold, degassed in a vacuum oven at 100°C for half an hour and moved to an air circulating oven to cure.

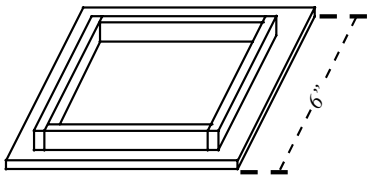

Fig. 1. Schematic diagram showing the mold used for curing the resin.

In the solvent process, the solution of the resin was mixed with other ingredients at room temperature, poured into the mold and placed in a vacuum oven at 100°C. The solvent was removed by applying vacuum and collected in a trap cooled by dry ice. When the solvent removal was complete, the mold with the resin was transferred to an air-circulating oven to cure. The same temperature sequence was followed for both processes: 70/24, 75/24, 80/24, 85/24, 90/24, 95/48, 110/24, 120/24, 130/48, 150/4, 175/4, 200/12, 230/6, and 260°C/8 h. At the end of this sequence a void free, fully cured plate 3.5–4 mm thick was obtained.

2.6. Characterization and testing

FT-IR. Transmission FTIR spectra were obtained by a Nicolet Magna-IR 860 Spectrometer. Liquids of relatively high viscosity were coated onto a KBr plate and low viscosity liquids were contained in a fixed liquid cell.

^{1}H-NMR. A 360 MHz spectrometer was used to collect ^{1}H spectra from a 50% sample solution in deuterated chloroform. TMS was used as reference and a 5 mm diameter NMR tube was used.

^{29}Si-NMR. ^{29}Si-NMR spectra were obtained from a 30% solution in chloroform-d_1 or benzene-d_6 using a Varian VXR-200 MHz spectrometer at 39.745 MHz. NMR tubes of sixteen mm in diameter produced by Wilmad Glass Co. were used. A pulse width of 12.4 μs and a relaxation delay time of 8 s were chosen. Chromium (III) acetylacetonate (0.03 M) was used as a paramagnetic relaxation agent.

GPC. The GPC column was packed with divinyl benzene crosslinked polystyrene beads of 5 μm in diameter and pore type mixed c supplied by Polymer Laboratory. The mobile phase was tetrahydrofuran and a refractive index detector was used. Polystyrene standards were used to determine the molecular weight.

Optical microscopy. A Zeiss optical microscope was used to take pictures of separate particles in an otherwise transparent casting.

SEM. Freshly fractured surfaces were observed under a Cambridge Instrument Stereoscan 240 SEM. The resin surfaces were coated with a thin layer of gold before observation and an acceleration voltage of 10–20 kV was used.

TGA. Thermal gravimetric analysis was done on a Seiko SSC/5200 TGA/DTA 320 system. Purging gas was air or argon flowing at 150 ml/min. The temperature was raised at 10°C/min from room temperature to 800°C. A single piece of material approximately 13.5 ± 0.2 mg in weight was used for each sample.

Three point bending test. The three point bending test was performed per ASTM standard D 790-92 [57]. The cured resin cast plates about 0.125–0.18 in. thick were cut into specimens 2 in. long and 0.5 in. wide and polished to reduce the thickness to 0.125–0.13 in. The specimens were polished further until smooth, and visible scratch free surfaces were obtained. This was done by using silicon carbide polishing papers in the following sequence: Grit # 320, 800, 1200, 2400, and 4000 and then water dispersed alumina powders of 1, 0.3 and 0.05 μm in diameter. All samples were polished through the same procedure to ensure a similar surface condition. The polished samples were dried at 80°C overnight and conditioned at the testing temperature and humidity for at least 24 h before testing. The test temperature was 21°C and a crosshead speed of 1 mm/min was used. The support span was 38 mm. For each sample at least three specimens were tested.

Fracture toughness testing. The plane strain fracture toughness, K_{Ic}, was obtained per ASTM D 5045-91a, and the critical strain energy release rate, G_{Ic}, was calculated from K_{Ic} based on LEFM assumptions [58–61]. The sample geometry, dimensions, and loading method are shown in Fig. 2. The single edge notch geometry was used. The cured cast plate was cut and six specimens 0.375 in. wide and 2 in. long were obtained. A 0.1 in. deep notch was cut by a diamond saw at the center of the specimen, and a natural crack extending from the root of the notch to about half of the width was produced by gently tapping a sharp razor blade into the notch. Samples were conditioned at room temperature for at least twenty-four hours before testing to allow full relaxation of deformation. The displacement rate of the test was 10 mm/min. For the geometry and loading conditions shown, with a support to width ratio of four,

$$K_{Ic} = [P/(BW^{1/2})]\, f(x) \tag{1}$$

where P is the highest load and:

$$f(x) = 6x^{1/2}[1.99 - x(1-x)(2.15 - 3.93x + 2.7x^2)] \\ /[(1+2x)(1-x)^{3/2}] \tag{2}$$

where x is the pre-crack to specimen width ratio, a/W. After the test the pre-crack length was measured. Only those specimens with a value between 0.45 and 0.55 were considered valid. The variation of x across the thickness should be less than 10%. The validity of the test was further ensured by comparing the sample dimensions with the estimated plastic zone size enlarged by approximately 25:

$$B, a, (W - a) > 2.5(K_{Ic}/\sigma_y)^2 \tag{3}$$

where σ_y is the yield stress of the sample.

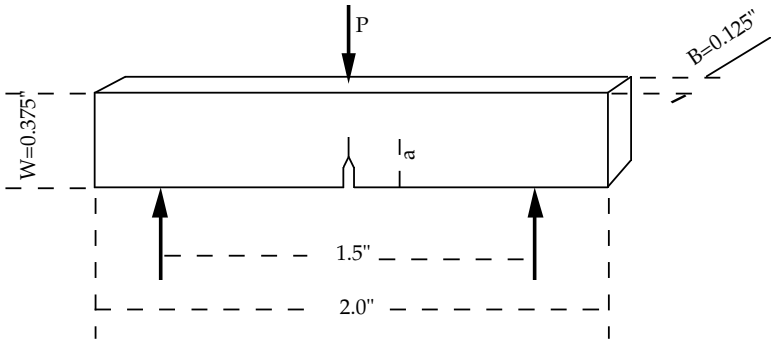

Fig. 2. Fracture toughness test sample geometry, loading position (P) and support positions (lower upward arrows).

From K_{Ic}, G_{Ic} was calculated by (Eq. (4)):

$$G_{Ic} = K_{Ic}^2(1 - \upsilon^2)/E \quad (4)$$

where υ, the Poisson's ratio of the resin, was neglected to simplify the experiment. For a glassy polymer with a typical Poisson's ratio of 0.3, G_{Ic} was exaggerated by about 9%. However, it was believed that the relative ranking of G_{Ic} values would not be obscured since the change of Poisson's ratio after toughening the resin was small.

3. Results and discussion

3.1. Preparation and characterization of functionalized PDMS

PDMS with a silanol termination was end capped with TEOS, as described below.

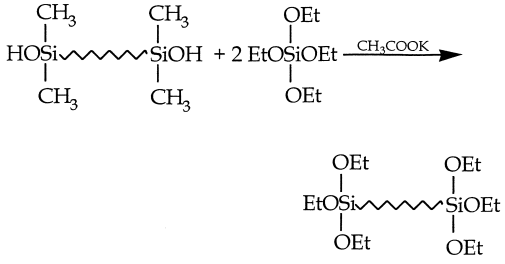

The silanol terminated PDMS was also end capped by phenyl trimethoxy silane. This end capped PDMS, however, was less often used, since its toughening effect was similar to that of the triethoxy siloxy version but it was much more difficult to prepare.

The IR absorption of silicones has been intensively studied [62–65]. References are available [66] which allow reliable assignments of absorption peaks. During the end capping reaction by TEOS it was used as a monitoring tool. The characteristic silanol absorption peak centered at 3312 cm^{-1} was used as an indication of whether or not the reaction was complete. The completion of the reaction was shown by the complete disappearance of this peak. Other changes in the IR spectrum after the reaction are also in agreement with a successful end capping. The absorption at ~900 cm^{-1}, of Si–O in SiOH, in addition to the 3312 cm^{-1} peak, disappeared. Two new absorption peaks attributed to the symmetric and asymmetric stretching of methylene at 2940 and 2885 cm^{-1}, and a characteristic, very strong absorption doublet at 1100–1080 cm^{-1}, of the stretching of the C–O bond of SiOEt, appeared. This characteristic doublet coincided with the antisymmetric stretching of Si–O–Si. At 1180 and 1068 cm^{-1} two absorption peaks of ethoxy group were also seen. The new peak at 1392 cm^{-1} was also consistent with an ethoxylated PDMS. Other absorption peaks due to the side methyl groups and the siloxane backbone either remained intact or overlapped with the new absorption peaks due to the ethoxy groups.

3.2. ^{29}Si and ^{1}H NMR

^{29}Si and ^{1}H NMR spectra of the triethoxy siloxy terminated PDMS of DP 14 are included in Fig. 3. The chemical shifts and their assignments are listed in Table 3 [64,67–75]. Triethoxy siloxy terminated PDMS of other degrees of polymerization had essentially similar spectra except the integral ratios of different nuclei.

In Fig. 3a, the ^{29}Si NMR spectrum of a triethoxy siloxyl terminated FB is shown. The end capping of FB, with a DP of 14, was achieved with minimum self-condensation and cyclization. No small cyclics were seen at −19.5 or −9.1 ppm. Silanol ends, originally at −11.5 ppm, were completely converted to triethoxy siloxy ends, appearing at −87.9 ppm. A small amount of self-condensation did occur but it only altered the degree of polymerization by 3%, from a theoretical value of 16 to an actual value of 16.5.

The structures of the triethoxy siloxy terminated PDMS were also verified by ^{1}H NMR. The ^{1}H NMR spectra of FBE and FCE are shown in Fig. 3b. The $SiCH_3$ proton coincided with the reference TMS. The $SiOCCH_3$ proton was at 1.1 ppm as a triplet and the $-CH_2-$ proton at 3.7 ppm as a quartet.

3.3. Ternary phase diagrams

Despite the compositional similarity, the 4-3136 resin

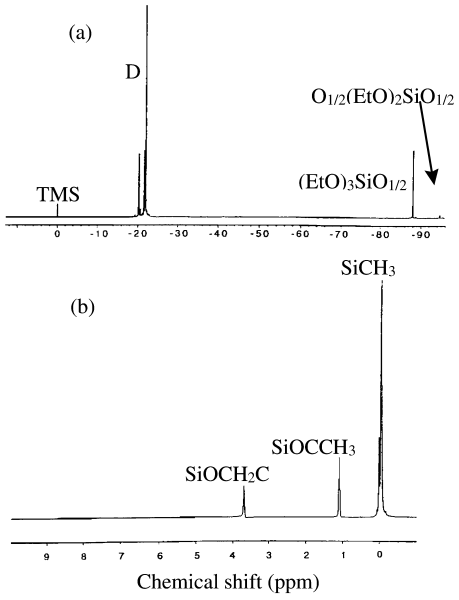

Fig. 3. (a) ^{29}Si. (b) ^{1}H NMR spectrum of triethoxy siloxy end capped FB.

pre-polymer and the PDMS short segments are incompatible due to their macromolecular nature. The liquid lattice theory [76] states that the free energy of mixing is:

$$\Delta F_M = kT[n_1 \ln v_1 + n_2 \ln v_2 + n_3 \ln v_3 + \chi_{12} n_1 v_2 + \chi_{13} n_1 v_3 + \chi_{23} n_2 v_3] \quad (5)$$

where ΔF_M is the free energy of mixing per unit volume of solution, n_i the number of molecules of the ith component in a unit volume of solution, v_i the volume fraction of the ith component in the solution, and χ_{ij} the pairwise interaction parameter which can be expected to be slightly positive. The structural and compositional differences contribute a positive value to the free energy of mixing and make the polymers incompatible. The entropy of mixing depends on the number of molecules, seen in the first three terms in Eq. (5). In the absence of a solvent, the numbers of polymer molecules, n_2 and n_3, are very small due to their polymeric nature, and the entropy of mixing is not enough to compensate for the small interaction difference between dissimilar molecules. As a result, a solvent is always needed to increase the entropy of mixing and to achieve a molecular mixing of the rubber segments with the resin. This is a prerequisite condition for an effective coupling reaction.

Phase diagrams of the 4-3136 resin/Toluene/PDMS system were constructed to define composition windows for a pre-coupling reaction. In Fig. 4, there is a small incompatible region at the right lower corner even when the DP of the PDMS chain is eight. The coupling reaction must be done outside this heterogeneous region. When the DP of the functionalized PDMS is increased to sixteen, the heterogeneous region is enlarged significantly. If the DP of the PDMS is 55 (FCE or FC), the boundary moves further up and the homogeneous region is even smaller. At room

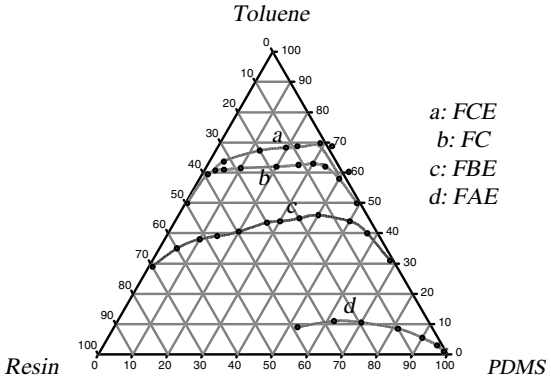

Fig. 4. Room temperature ternary phase diagrams of the resin/toluene/PDMS.

temperature, the FCE and 4-3136 resin can be compatiblized only in a toluene solution of concentration below 35 wt%. However, for this system the coupling reaction was actually done at 95°C in a 38 wt% solution regardless of the ratio of FCE to the resin. It was expected that the elevated temperature lowered the boundary curve on the phase diagram by a few percent.

The phase diagram also shows the FCE was made less compatible with the 4-3136 resin by triethoxy siloxy end capping. In subsequent studies the incompatibility of the 4-3136 resin and the PDMS was utilized to control second phase morphology.

3.4. Coupling reaction of the PDMS segments with the resin

There are several ways to incorporate the functionalized PDMS into silicone resin networks. The mechanical properties and fracture toughness are the criteria to determine the more appropriate route.

The coupling of the PDMS and the resin was done in toluene with 0.1–0.4% titanium tetrabutoxide, at a temperature between 95 and 105°C. The concentration of the mixture was the most important factor affecting reaction efficiency. The resin oligomer and the rubber segments must achieve molecular mixing for the reaction to proceed; otherwise phase separation occurs, and effective coupling is not accomplished. The phase diagrams were used to define a composition window in which molecular mixing could be achieved. It was found that the functionalized PDMS and resin oligomers were effectively compatiblized when the reaction was done in a concentration in the homogeneous region in the phase diagram, elsewhere, opaque castings were always obtained containing separate phase domains larger than 1 μm.

^{29}Si NMR. The ^{29}Si NMR spectra, in Figs. 5 and 6, showed that: (1) a catalyst and an elevated temperature were needed for the coupling reaction; (2) the reaction temperature should not be excessively high, otherwise the removal of volatile substances would diminish the reaction efficiency; and (3) when done correctly, the functionalized PDMS segments were completely coupled with the resin.

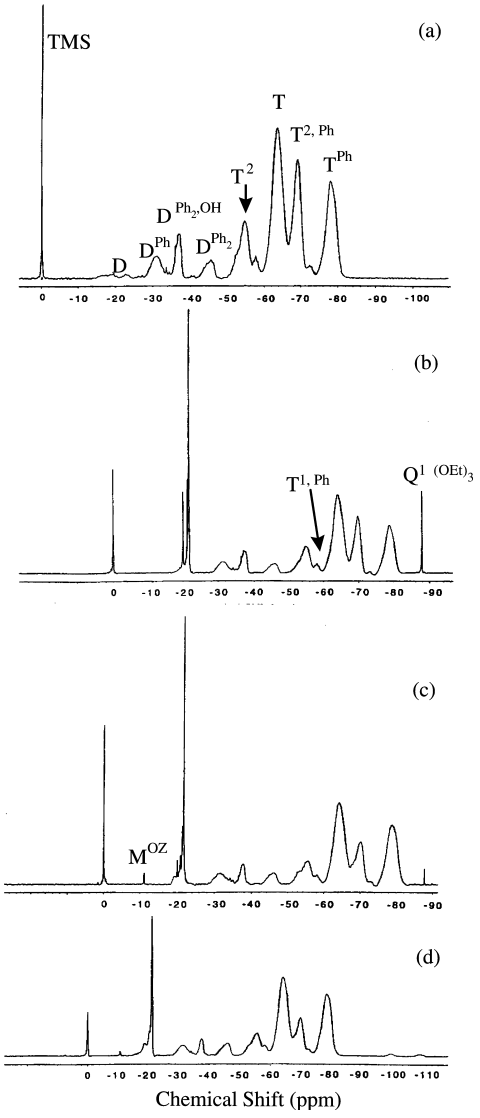

Fig. 5. ^{29}Si NMR spectra of (a) the resin; (b) a mixture of the resin with 10 parts of FBE without the pre-coupling reaction; (c) the resin coupled with 10 parts of FBE, volatile substances were removed from the beginning of the reaction; and (d) the resin coupled with 20 parts of FBE, no volatile substances were removed from the reaction.

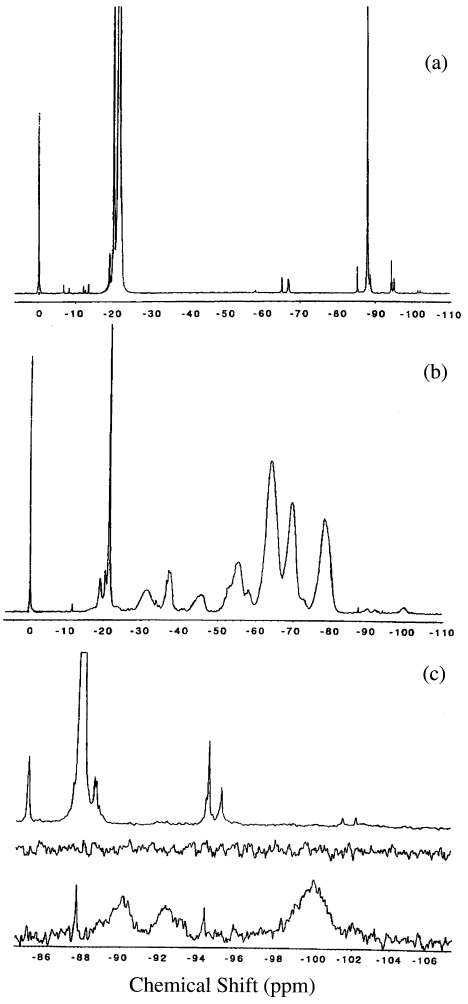

Fig. 6. ^{29}Si NMR spectra (a) of FBE after being heated at 105°C for 28 h with 0.1 wt% $Ti(OBu)_4$, (b) of the resin coupled with 10 parts of FBE. The coupling reaction was partially finished, and (c) selected regions of Fig. 6(a) (top), Fig. 5(a) (middle); and Fig. 6(b) (bottom).

The chemical shifts of peaks appearing in Figs. 5 and 6 and their assignments are listed in Table 4. In addition to the positions of peaks, linewidth also provides useful information. Silicon nuclei in the PDMS segments usually have narrow peaks on the spectra (Fig. 6a), while those in the resin oligomer show a much broader linewidth, due to the multiplicity of their environment (Fig. 5a). For the same reason, when the PDMS ends are coupled with resin oligomers the resonance peaks of these end nuclei become very broad (Fig. 5d peaks in the −100 to −110 ppm region). This serves as a means to distinguish between the PDMS reaction with itself and with the resin.

The spectrum of the resin is shown in Fig. 5a. The starting compositions of the resin and those calculated from the NMR spectrum are listed in Table 5. At the resin stage, a higher fraction of methyl T monomer was converted to T network structure than phenyl T monomer due to less steric hindrance. This led to the compositional and crosslink density heterogeneity in the final cured network. Approximately one third of the silicon atoms from $MeSiCl_3$, half of those from $PhSiCl_3$, the majority of those from Ph_2SiCl_2, and a negligible number of those from $PhMeSiCl_3$ retained one or two uncondensed hydroxyl groups available for the subsequent coupling reaction.

The spectrum of a mixture of the resin and 10 parts of FBE, shown in Fig. 5b, was simply the superposition of the resin spectrum and the FBE spectrum. Without catalysts and elevated temperatures, no coupling reaction between FBE and the resin occurred.

In the presence of titanium tetrabutoxide, and at an elevated temperature, the functionalized PDMS and the

Table 4
^{29}Si chemical shifts and their assignments (R stands for an unspecified alkyl)

δ (ppm)	Assignment	Notation	Comments
0	Me_4Si		Reference
−9.51	$(Me_2SiO)_3$	D_3	
−11.1	$O_{1/2}(Me)_2SiOZ$	D^{oz}	Z = H or R
−19.8 to −21.6	$O_{1/2}Si(Me_2)O_{1/2}$	D	
−22.8	$PhMe(OH)SiO_{1/2}$	$D^{Ph,\ OH}$	
−31.1	$O_{1/2}Si(PhMe)O_{1/2}$	D^{Ph}	Broad peak
−37.4	$O_{1/2}Si(Ph_2)OH$	$D^{Ph_2,\ OH}$	Broad peak
−41.0	$O_{1/2}Si(Ph_2)OR$	$D^{Ph_2,\ OR}$	Trace
−45.9	$O_{1/2}Si(Ph_2)O_{1/2}$ or $O_{1/2}Si(Me)(OH)_2$	D^{Ph_2} T^1	Broad peak
−54.8	$O_{1/2}Si(Me)(OH)O_{1/2}$	T^2	Broad peak
−58.1	$O_{1/2}Si(Ph)(OH)_2$	$T^{1,\ Ph}$	Broad peak
−63.9	$MeSiO_{3/2}$	T^3	Broad peak
−69.9	$HOSi(Ph)O_{2/2}$	$T^{2,\ Ph}$	Broad peak
−72.1	$ROSi(Ph)O_{2/2}$	$T^{Ph,\ OR}$	Broad peak
−78.7	$PhSiO_{3/2}$	$T^{3,\ Ph}$	Broad peak
−85.1	$O_{1/2}Si(OEt)_2OH$	$Q^{1,\ (OEt)_2}$	Narrow
−87.8	$O_{1/2}Si(OEt)_3$	$Q^{1,\ (OEt)_3}$	Narrow peak
−90.3	$EtO(OH)SiO_{2/2}$	$Q^{2,\ OEt}$	Broad peak
−92.3	$(EtO)_2SiO_{2/2}$	$Q^{2,\ (OEt)_2}$	Broad peak
−94.3	$O_{1/2}Si(OH)_2O_{1/2}$	Q^2	From self condensation of −Si(OEt)$_3$
−95.2	$O_{1/2}Si(OEt)_2O_{1/2}$	$Q^{2,\ (OEt)_2}$	From self condensation of −Si(OEt)$_3$
−101.6	$HOSiO_{3/2}$	Q^3	Same as above
−102.2	$EtOSi_{3/2}$	$Q^{3,\ OEt}$	Same as above
−110	$SiO_{4/4}$	Q^4	Broad

resin were coupled. The reaction efficiency was affected by a variety of factors including the reactant concentration, the catalyst level, and whether or not volatile materials were removed from the reaction system.

The spectra in Fig. 5c and d show the effect of removing volatile materials. Fig. 5c was a spectrum for the resin coupled with 10 parts of FBE, when the reaction was done at 105°C with 0.1 wt% $Ti(OBu)_4$, and volatile substances were removed from the beginning of the reaction. The removal of volatile substances was controlled by sweeping nitrogen gas. A substantial amount of the triethoxy siloxy ends remained unreacted, indicated by the remaining peak at −87.8 ppm in Fig. 5c. If no volatile substances were removed and the other reaction conditions kept the same, the triethoxy siloxy peak disappeared completely (Fig. 5d), indicating a complete coupling reaction. The absence of peaks in the region from −90 to −95 ppm indicated that at least two of the three ethoxy groups at each end reacted with the resin. This was also shown by the appearance of the −100 ppm and −110 ppm peaks, respectively, for ends with two and three ethoxy groups reacted.

The IR spectra of condensed volatile substances were consistent with a mixture of water and ethanol, indicating condensation of resin terminal silanols with themselves, and condensation between resin terminal silanol and the PDMS

Table 5
Compositions of the resin

Starting material	Quantity (mol%)	Structure in resin shown by NMR	Notation	Quantity (mol%)
$MeSiCl_3$	45	$MeSiO_{3/2}$	T^3	32.4
		$O_{1/2}Si(Me)(OH)O_{1/2}$	T^2	10.5
		$O_{1/2}Si(Me)(OH)_2$	T^1	<2.7
$PhSiCl_3$	40	$PhSiO_{3/2}$	$T^{3,\ Ph}$	20.1
		$HOSi(Ph)O_{2/2}$	$T^{2,\ Ph}$	19.6
		$ROSi(Ph)O_{2/2}$	$T^{2,\ Ph,\ OR}$	1.4
		$O_{1/2}Si(Ph)(OH)_2$	$T^{1,\ Ph}$	2.3
Ph_2SiCl_2	10	$O_{1/2}Si(Ph_2)O_{1/2}$	D^{Ph_2}	<2.7
		$O_{1/2}Si(Ph_2)OH$	$D^{Ph_2,\ OH}$	5.0
		$O_{1/2}Si(Ph_2)OR$	$D^{Ph_2,\ OR}$	0.5
$PhMeSiCl_2$	5	$O_{1/2}Si(PhMe)O_{1/2}$	D^{Ph}	4.6
		$PhMe(OH)SiO_{1/2}$	$D^{Ph,\ OH}$	0.3

terminal groups. The removal of ethanol may facilitate the condensation between the PDMS terminal ethoxy with the resin silanol, but the removal of water promoted the condensation of resin silanols with themselves and diminished the number of reaction sites on the resin and led to a less efficient coupling reaction. During the coupling reaction, small amounts of side reactions occurred. For example, the peaks at −19.3 ppm and −11.2 ppm may suggest the appearance of cyclic structures and dimethyl silanol ends (−$OSiMe_2OH$) as a result of the re-equilibration of PDMS chains, though the extent was negligible.

That the triethoxy end groups reacted mostly with the resin oligomer instead of PDMS was further supported by a sluggish self-condensation observed by NMR. In a ^{29}Si NMR spectrum the peaks for the PDMS chain ends coupled with resin oligomers were broad due to the multiplicity of their environment, whereas self condensation of rubber segments gave very narrow, well defined peaks (Fig. 6a). The spectrum in Fig. 6a is for a pure FBE sample after being subjected to the same heat history as a coupling reaction with the catalyst. Mostly the FBE remained intact. The observed trace reactions included the self-condensation, the re-equilibration of PDMS, and the substituent redistribution. Less than 4% of the total functional ends participated in the self-condensation. A trace amount of re-equilibration occurred and the appearance of T units revealed the redistribution of a small number of methyl groups.

Effective coupling can be more clearly shown by the NMR spectrum of a reaction in progress (Fig. 6b). The useful region of Fig. 6b was re-plotted with the same region of the FBE and the resin spectra (Fig. 6c). In Fig. 6c, the top spectrum was for pure FBE, the middle for the resin oligomer, and the bottom for the coupled resin/PDMS. After partial reaction, the −87.8 ppm peak had almost disappeared. Broad peaks appeared: at −90 ppm, for the PDMS ends with one ethoxy group reacted with the resin and another hydrolyzed; at −92.3 ppm, for

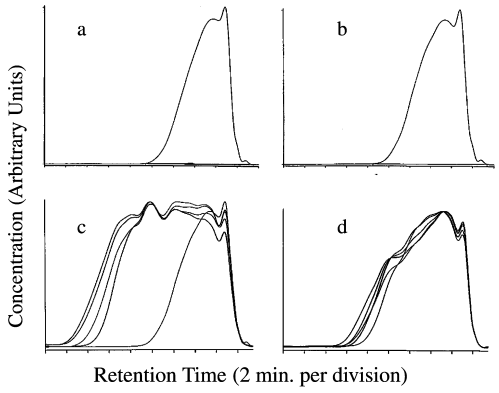

Fig. 7. GPC retention time vs. concentration curves: (a) the resin; (b) the mixture of the resin with 10 parts of FBE without the pre-coupling reaction; (c) the resin coupled with different modifiers in solutions of different concentrations. The modifiers and reaction solution concentrations were, from right to left: no modifier; 10 parts of FBE, 46 wt%; 10 parts of FBM, 65 wt%; 10 parts of FBE, 51 wt%; 20 parts of FBE, 53 wt%; and (d) the resin coupled with different amounts of FCE. The amounts of FCE were, from right to left: 5, 10, 15, and 20 parts.

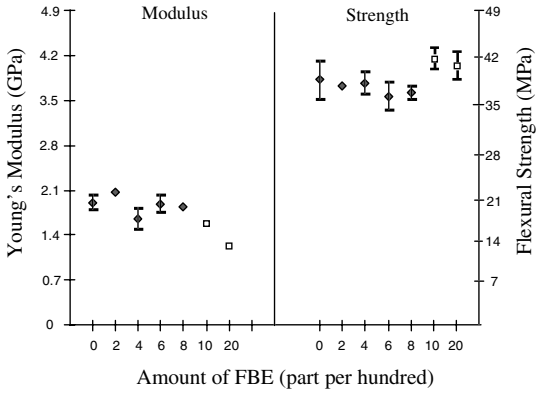

Fig. 8. Flexural properties of the network co-cured with FBE or pre-coupled with FBE and then cured. Some data points do not have error bars since their error bars are buried in the marks that indicate average value.

those with one ethoxy group reacted with resin and the other intact; and at −100 ppm, for those with two ethoxy groups reacted with the resin and the other one hydrolyzed.

3.5. GPC analysis

Despite the uncertainty caused by the use of the polystyrene standards, GPC was a useful tool to qualitatively evaluate the hydrodynamic size of the resin molecules and their distribution. In Fig. 7 are plotted the GPC column retention time vs. concentration curves. The weight concentration is represented by the vertical axis which corresponds to the refractive index difference between the reference and the sample.

Fig. 7a is for the neat 4-3136 resin. The curve consists mainly of three peaks, the overlapping peaks at 17.5 and 18.2 min, and a small peak at 19.5 min. Fig. 7b is for a mixture of the resin with 10 parts of FBE. The mixture was not heated, and there was essentially no coupling reaction between the resin and the PDMS, according to the NMR spectrum. The FBE was concealed by the resin peaks.

After a coupling reaction the molecular weight was increased and its distribution broadened (Fig. 7c). In Fig. 7c, the GPC curves of the resin, and the resin reacted with different amounts of FBE or FBM (dimethoxy siloxy terminated FB), are plotted. From the left to the right, the curves in Fig. 7c correspond to samples 3, 5, 6 and 4 in Table 6. The small peak on the far right side of the curve, for the lowest molecular weight species of the resin, disappeared after the coupling reaction, and the height of the next low molecular weight peak was reduced. The curves generally expanded in the high molecular weight direction.

The GPC curves of the resin coupled with FCE are plotted in Fig. 7d. From the left to the right, the curves in Fig. 7d are for the resins coupled with 20, 15, 10, 10, and 5 wt% FCE. Again the reaction of FCE with the resin increased the molecular weight and broadened the molecular weight distribution. Because of the higher molecular weight of FCE, fewer resin blocks were coupled with the PDMS

Table 6
Average molecular weight and its distribution, from GPC, of 4-3136 resin coupled with functionalized PDMS

Code	Toughener	Reaction	M_n	M_w/M_n
1	None	None	1410	1.805
2	10 Parts of FBE	None	1507	2.013
3	10 Parts of FBE	108°C, 28 h, 53 wt%[a]	3312	15.64
4	10 Parts of FBE	108°C, 28 h, 46 wt%	3109	7.535
5	20 Parts of FBE	108°C, 28 h, 51 wt%	3237	13.99
6	10 Parts of FBM	108°C, 28 h, 65 wt%	3121	10.11
7	5 Parts of FCE	95°C, 28 h, 38 wt%	2158	3.205
8	10 Parts of FCE	95°C, 28 h, 38 wt%	2310	3.990
9	15 Parts of FCE	95°C, 28 h, 38 wt%	2311	4.617
10	20 Parts of FCE	95°C, 28 h, 38 wt%	2327	5.545

[a] In toluene solution.

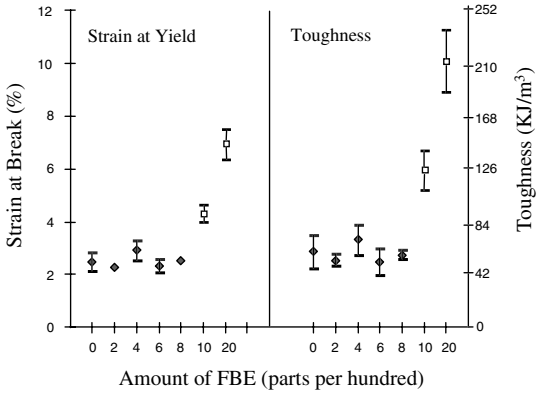

Fig. 9. Flexural properties of the network co-cured with FBE or pre-coupled with FBE and then cured. Some data points do not have error bars since their error bars are buried in the marks that indicate average value.

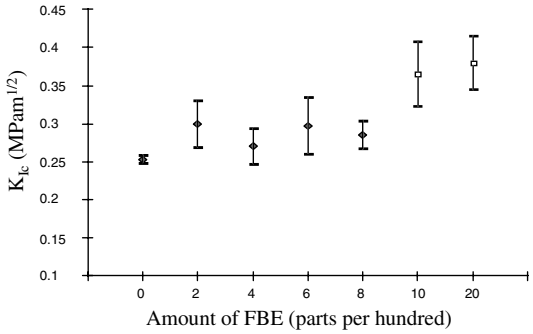

Fig. 10. K_{Ic} of the network modified with FBE through co-curing or pre-coupling.

ends and only a small increase in the average molecular weight was measured. The molecular weight distributions were broadened but generally they were much narrower than the resin reacted with FBE.

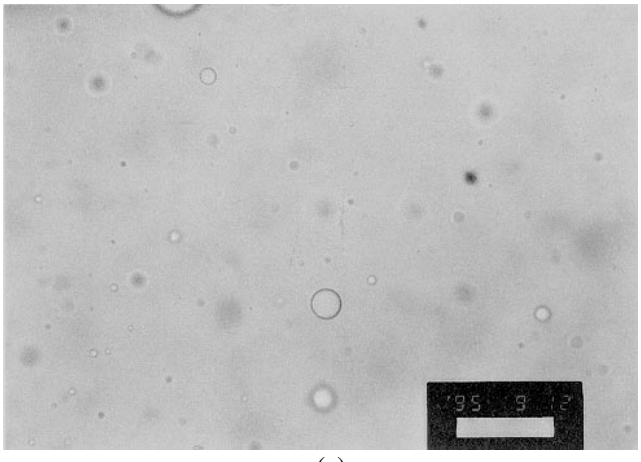

(a)

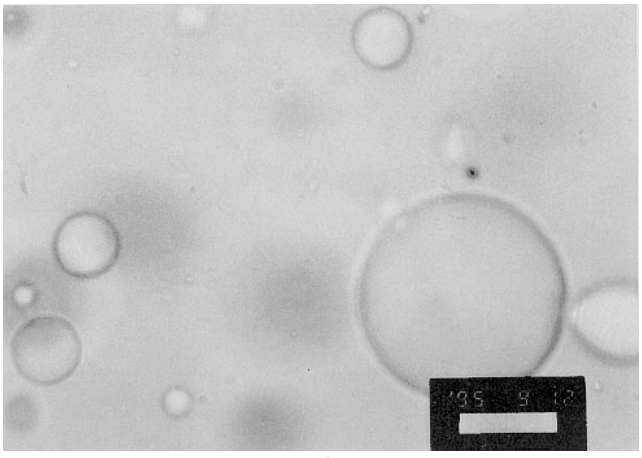

(b)

Fig. 11. Optical microscopy pictures taken from inside a cured network co-cured with: (a) 2 parts of FBE; and (b) 8 parts of FBE. Magnification: 333×.

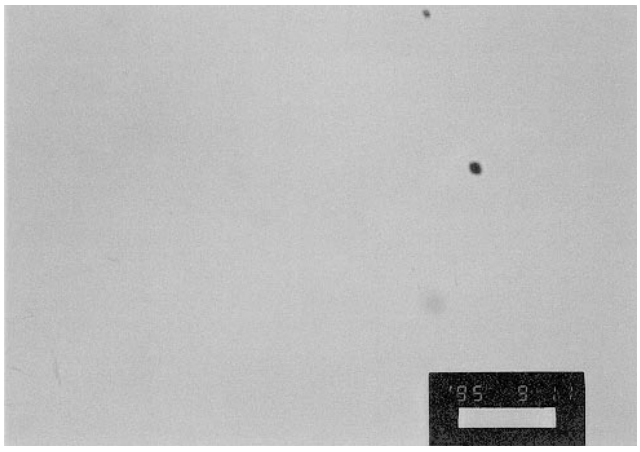

Fig. 12. Optical microscopy picture taken from inside a cured network pre-coupled with 10 parts of FBE. The casting was transparent and the black spots were impurities. Magnification: 333×.

3.6. Pre-coupling vs. co-curing

The simplest way to incorporate the tougheners into a network is mixing the resin with the tougheners and co-curing them. This is what has been often practiced for epoxy resins. Whether or not such a simple route is suitable here is investigated by comparing the mechanical properties of the cured networks from this route and from the pre-coupled route. Cast plates were made from the resin pre-coupled and co-cured with FBE and tested. The results are plotted in Figs. 8–10. The solid diamonds in the figures are the data obtained from co-cured samples and the open squares from the pre-coupled ones. When 2 to 8 parts (per 100 parts of resin) of FBE was co-cured with the resin the networks showed essentially no change in mechanical properties. When pre-coupled with the resin and then cured, however, 10 and 20 parts of FBE significantly improved the fracture toughness and strain at break of the network,

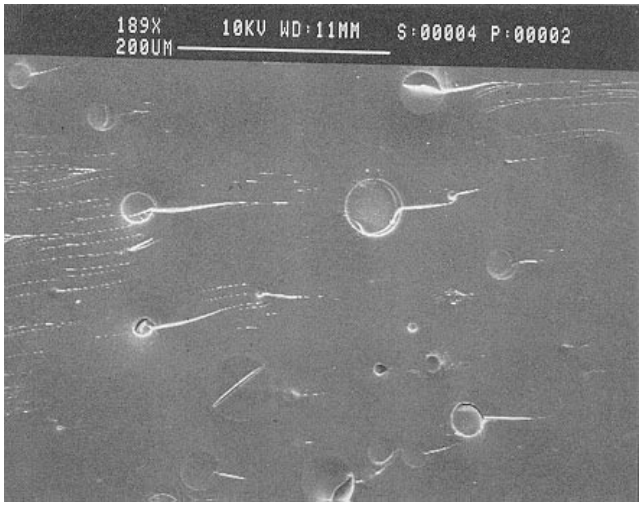

Fig. 13. SEM photo taken from the freshly fractured surface of networks co-cured with 8 parts of FBE, showing second phase particles.

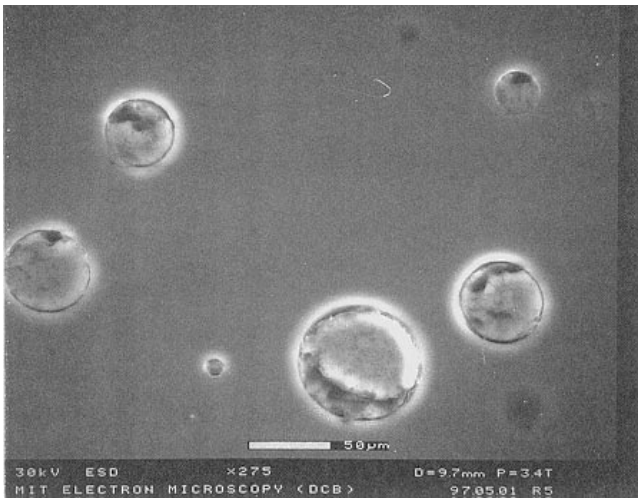

Fig. 14. Photos taken by an Environmental SEM from the polished surface of a network co-cured with 8 parts of FBE, showing second phase particles.

while the strength was slightly increased and modulus slightly reduced.

In a co-cured system, FBE was not well compatiblized with the resin due to the poor coupling reaction. In Fig. 11a, separate particles were seen when FBE was co-cured, in contrast to a homogeneous casting when the FBE was pre-coupled (Fig. 12). By a co-curing process more FBE produced larger particles (Fig. 11b). The presence of particles was also verified by SEM observation of the freshly fractured surface (Fig. 13). The particles contracted more than the matrix after cooling and appeared as depressions on the fractured surface. They were flat on a polished surface (Fig. 14) and the rubbery composition of these particles was verified by EDS analysis. The separate particles had no toughening effect in the cured brittle matrix. The pre-coupling step was therefore necessary.

3.7. Mechanical properties of the toughened networks

The ethoxylated PDMS short segments were pre-coupled with the 4-3136 resin and cast plates of them were cured. Specimens were cut from the plates and tested, according to the procedures described. The results are shown in Figs. 15–20.

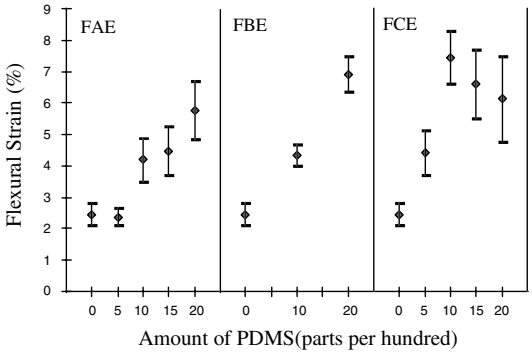

Fig. 15. Flexural strain of the networks modified by pre-coupling with functionalized PDMS of various chain lengths.

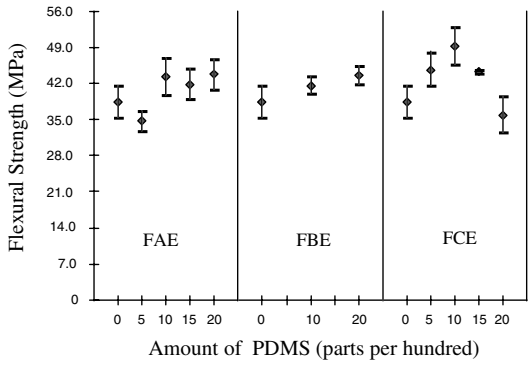

Fig. 16. Flexural strength of the networks modified by pre-coupling with functionalized PDMS of various chain lengths.

The unmodified 4-3136 resin had a strain at break of 2.46%, a Young's modulus of 1.88 GPa, a flexural strength of 37.73 MPa, and a toughness value, measured by the area under the stress–strain curve, of 5.9 kJ/m^3. These values are low compared to most untoughened epoxy resins. The K_{Ic} value of the unmodified 4-3136 resin was 0.253 MPa m$^{1/2}$, and the G_{Ic} value 34.05 J/m^2. Both are less than half of most untoughened epoxy resins.

All functionalized PDMS short chains toughened the 4-3136 resin when they were incorporated through the pre-coupling reaction. In Figs. 15–20, they increased the strain to break and the integral area under the stress–strain curve. The flexural strength also increased slightly. The Young modulus dropped slightly. At the optimal composition, with 10 parts of FCE, the fracture toughness, K_{Ic}, was increased from 0.253 to 0.459 MPa m$^{1/2}$, and the critical strain energy release rate, G_{Ic}, was increased from 34.05 to 151.11 J/m^2. The Young modulus was decreased from 1.88 to 1.37 GPa.

Longer PDMS chains are more effective than shorter ones. With a DP of 8, 10 parts of FAE improved the ultimate strain by 70%, the flexural strength by 13%, the K_{Ic} by 23%, and the G_{Ic} by 135%. With a DP of 55, 10 parts of FCE increased these properties by 202, 28.5, 80, and 350%,

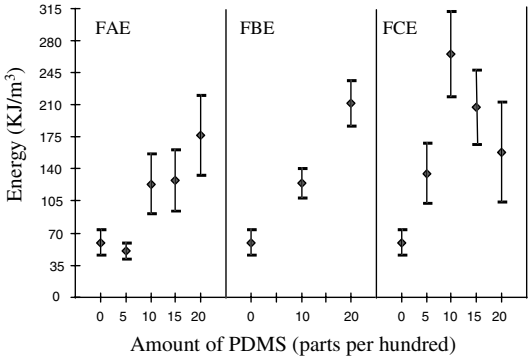

Fig. 17. Toughness measured by the area under the stress–strain curve of the networks modified by pre-coupling with functionalized PDMS of various chain lengths.

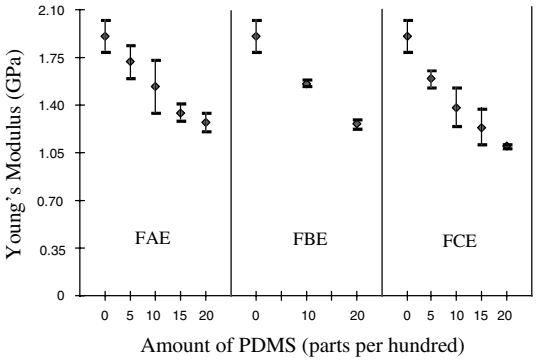

Fig. 18. Young's modulus of the networks modified by pre-coupling with functionalized PDMS of various chain lengths.

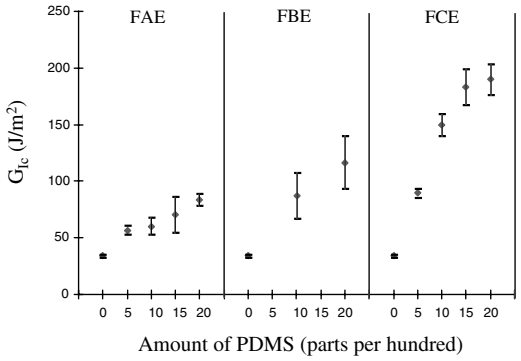

Fig. 20. G_{Ic}, the critical strain energy release rate, of the networks modified by pre-coupling with functionalized PDMS of various chain lengths.

respectively. Longer chains also caused a slightly larger drop in modulus. When the DP of the PDMS was 16, in between 8 and 55, the cured network properties were also in between. In Figs. 15–20, a longer PDMS chain caused an increasing rate of property change with the PDMS content. This behavior was attributable to the mobility of the PDMS chains which were linked to the resin network by their reacted ends. A long chain, such as the FCE with a DP of 55, is less restricted and freer to move when stressed, whereas the shorter ones are more constrained. This is evidenced by the shift of the PDMS relaxation peaks on a DMA spectrum and will be discussed in a separate paper. The longer PDMS segment is more effective in promoting mechanical energy dissipation of the entire network. The combination of higher mobility of the PDMS chains and the more effective promotion of flow in the surrounding matrix makes the longer PDMS segments better tougheners.

In Figs. 15–17, and 19 and 20, a maximum in the corresponding mechanical properties is seen at 10 parts of FCE, after which the strain, the strength, and the area under the stress–strain curves dropped, while the K_{Ic} and G_{Ic} continued to increase, but at a smaller rate. It is suggested that this is caused by the higher residual stress in the formulations containing more FCE. This stress was verified by viewing the cross section of a resin casting with crossed polarizers, as well as by the behavior of castings when a pre-crack was made. In polarized light, birefringence was seen in the directions along the surfaces in the areas close to both surfaces. It was absent in the unmodified resin and very slight in the shorter chain PDMS toughened resins. When a razor blade was tapped into the notch to make a pre-crack, with an increasing amount of FCE, the samples became increasingly prone to crack from surfaces, consistent with a tensile residual stress at the surfaces.

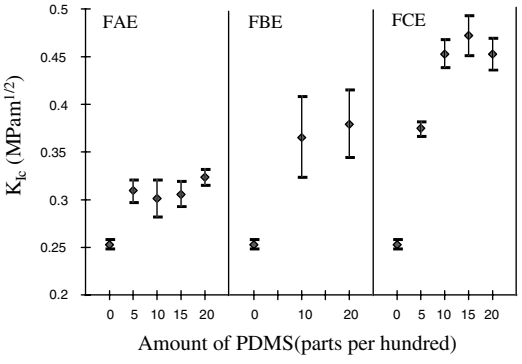

Fig. 19. K_{Ic}, the fracture toughness, of the networks modified by pre-coupling with functionalized PDMS of various chain lengths.

3.8. Thermal stability of the toughened networks

Rubber modification in a polymer often results in degradation of its thermal resistance, because usually the rubbers are less thermally stable. Heat resistant rubbers are desirable when such properties are critical for the modified polymer. Although better than most rubbers, PDMS is known to undergo thermal depolymerization and to form small cyclic species [77–80] through siloxane bond intramolecular or intermolecular interchange, which involves a four-center transition state [81]. Intermolecular interchange involves two siloxane chains, while intramolecular interchange requires that a single chain folds and forms the transition-state. The comparative thermal stability of the toughened networks was investigated using TGA. No difference was detected between the FAE toughened and the untoughened networks. However, a small degradation was detected when the DP of the PDMS became larger. It has been reported that PDMS undergoes a rapid depolymerization above 350°C [77–80]. It seems this was hindered first by the dispersion of the PDMS chains in a silsesquioxane network, and second by shortening the chain length. The dispersion of PDMS in a silsesquioxane network diminished the probability of siloxane bond intermolecular exchange, while the shorter chain length makes it more difficult to fold a single chain when it is anchored on both ends in a rigid network.

3.9. Fractography

The fracture surface morphology of the cured network depends on the position and shape of the initial crack, the loading rate and geometry, the resin composition, and morphology. An analysis of these features helps reveal the

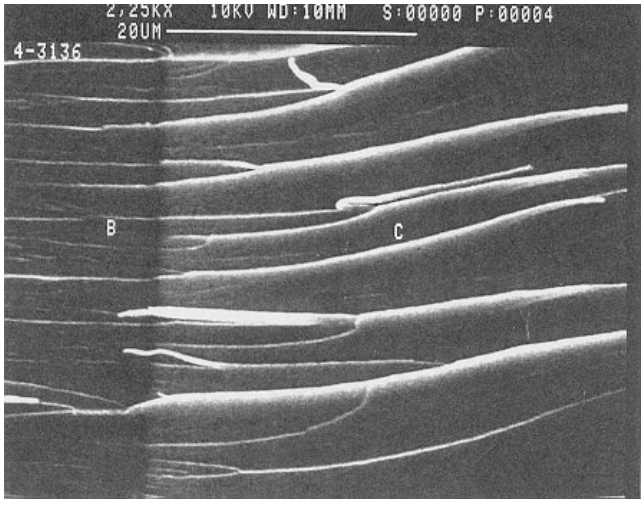

(a)

(b)

Fig. 21. SEM photos taken after a fracture toughness test from the fractured surfaces of: (a) the untoughened network; and (b) a network toughened by 10 parts of FCE. Crack travels from the left to the right.

toughening mechanism. Preston [82,83] showed that in a brittle solid a crack moves perpendicular to the direction of the principle tension. This simple rule has been observed in a great variety of brittle materials and is widely accepted. A change of fracture path is a result of the rotation of the principle tension direction. The direction of the principle tension can rotate in at least two ways: around an axis parallel to the crack advance direction in the crack plane; or around an axis perpendicular to it in the crack plane. The former is called a twist and the latter a tilt. A tilt produces multi crack planes parallel to the main crack plane but at different elevations, and a twist produces serrated multi crack planes forming an angle with the main crack plane. Fig. 21a, a SEM picture of the fractured surface of the unmodified network, shows such features of essentially brittle fracture. Serrated multi planes already existed in the pre-crack (area B) and such cracking pattern was

Table 7
Calculated plastic zone size in the 4-3136 network

Toughener	K_{Ic} (MPa m$^{1/2}$)	σ (MPa)	r_y (μm)
None	0.253	37.732	2.4
5 Parts of FAE	0.310	34.113	4.4
10 Parts of FAE	0.301	42.633	2.8
15 Parts of FAE	0.306	41.172	2.9
20 Parts of FAE	0.324	43.054	3.0
5 Parts of FBE	0.285	48.251	1.9
10 Parts of FBE	0.328	40.917	3.4
15 Parts of FBE	0.333	44.115	3.0
20 Parts of FBE	0.380	41.006	4.6
5 Parts of FCE	0.375	43.964	3.9
10 Parts of FCE	0.453	48.492	4.6
15 Parts of FCE	0.473	43.516	6.3
20 Parts of FCE	0.453	35.368	8.7

essentially undisturbed when the crack was re-initiated. Thereafter, some sub planes merged and fewer such planes were seen (area C). When a sharp crack is subjected to an opening force the stress singularity at the tip is relieved by plastic deformation of the material around it. The capability of a material to sustain such a stress without catastrophic failure, the fracture toughness, is directly related to the yielding around the crack tip which blunts the tip radius. According to Irwin's correction [84], for plane strain, the radius of the plastic zone can be estimated by:

$$r_y = \frac{1}{6\pi}\left(\frac{K_{Ic}}{\sigma_{ys}}\right)^2 \tag{6}$$

where r_y is the radius of the plastic zone, and σ_{ys} the yield stress. Since classical yielding has not been observed in the network, the flexural stress at break is used to approximate σ_{ys}. The values so calculated are presented in Table 7, and they show that the plastic zone increases as the PDMS toughens the material.

Fig. 21b, a SEM fractograph of the network toughened by 10 parts of FCE, shows a highly deformed zone. This was identified as the process zone when the crack was stressed during the first part of the fracture toughness test since the position of this zone was behind the tip of the pre-crack and just ahead of the unstable crack. No similar feature was found beyond this zone, suggesting that crack speed plays an important role in determining the scale of plastic deformation.

4. Conclusions

Polysilsesquioxane networks are very brittle materials but can be substantially toughened by homogeneous incorporation of PDMS segments. The strain at break, the area under the stress–strain curve, the strength, the fracture toughness K_{Ic}, and the critical strain energy release rate G_{Ic} are increased after toughening, while the Young's modulus is slightly decreased. When homogeneously incorporated, longer PDMS chains are more effective tougheners, due to

their higher mobility and their ability to more effectively promote plastic deformation in the entire network. It has been identified that the enhanced inelastic deformation is responsible for the increased fracture toughness.

The compatibility of the PDMS and the investigated silsesquioxane resin is dependent on the chain length of the PDMS. Longer chains are less compatible with the resin. To incorporate PDMS short chains into a polysilsesquioxane network a pre-coupling step before curing is needed. Otherwise PDMS phase separated domains form which do not toughen the network.

The thermal stability of the polysilsesquioxane network is relatively well retained after PDMS toughening, although longer chain PDMS tends to degrade it slightly more than shorter ones.

References

[1] Hourston DJ, Lane S, Zhang HX. Polymer 1991;32:2215.
[2] Sullivan VJ. ANTEC ’93, May 1993, 96p.
[3] Chung JYJ, Lazear NR. ANTEC ’94, May 1994, San Francisco, 1728p.
[4] Chung M-F, Golovoy A, Mindroiu VE, Plummer HK, van Oene H. Polymer 1993;34:3809.
[5] Kramer EJ. M MM Press Symposium Series: Polymer Compatibility and Incompatibility, Principles and Practices: Papers Presented at the 10th Midland Macromolecular Meeting, vol. 2, Midland, MI, MMM Press by Harwood Acedamic Publishers, New York, 1982. 251p.
[6] McGarry FJ. In: Arends CB, editor. Polymer toughening, New York: Marcel Dekker, 1989 (175p).
[7] Huang Y, Hunston DL, Kinloch AJ, Keith RC. Rubber toughened plastics, ACS Advances in Chemistry Series 233. Washington, DC: American Chemical Society, 1993 (p. 1).
[8] Bucknall CB. Toughened plastics. London: Applied Science, 1977.
[9] Seymour RB. In: Riew CK, editor. Rubber toughened plastics, ACS Advances in Chemistry Series 222Washington, DC: American Chemical Society, 1989.
[10] Hedrick JL, Allen RD, Diaz A, Hilborn JG, Hendrick JC. Polym Bull 1993;31:715.
[11] Majumdar B, Keskkula H, Paul DR. Polymer 1994;35:1399.
[12] Kumar G, Neelakantan NR, Subramanian N. J Mater Sci 1995;30:1480.
[13] Hobbs SY, Bopp RC, Watkins VH. Polym Engng Sci 1983;23:380.
[14] Arends CB, editor. Polymer toughening New York: Marcel Dekker, 1989.
[15] Koo KK, Inoue T, Miyasaka K. Polym Engng Sci 1985;25:741.
[16] Angola JC, Fujita Y, Sakai T, Inoue T. J Polym Sci, Part B: Polym Phys 1988;26:807.
[17] Kurauchi T, Ohta T. J Mater Sci 1984;19:1699.
[18] Karger-Kocsis J. Polym Bull 1996;36:119.
[19] Konczol L, Doll W, Michler GH. Colloid Polym Sci 1992;270:972.
[20] Narisawa I. 190th ACS National Meeting, Division of Polymer Chemistry, Chicago, September 1985, paper 122.
[21] Argon AS, Cohen RE, Qin J. 190th ACS National Meeting, Division of Polymeric Materials: Science and Engineering, Inc., August 1985, paper 1.
[22] Qin J, Argon AS, Cohen RE. 190th ACS National Meeting, Division of Polymeric Materials: Science and Engineering, Inc., August 1985, paper 2.
[23] Okamoto Y, Miyagi H, Uno T, Amemiya Y. Polym Engng Sci 1993;33:1606.
[24] Cheng C, Hiltner A, Baer E, Soskey PR, Mylonakis SG. J Appl Polym Sci 1994;52:177.
[25] Ishikawa M. Polymer 1995;36:2203.
[26] Sultan JN, McGarry FJ. Microstructural characteristics of toughened thermosett polymers, MIT School of Engineering, Research Report R69-59, October 1969.
[27] Zhu B. PhD dissertation, M.I.T., September 1997, Cambridge, MA.
[28] Selsing J. J Am Ceram Soc.—Discuss Notes 1961;August:419.
[29] Lawn BR, Wilshaw TR. Fracture of brittle solids, 1975. Cambridge: Cambridge University Press, 1933 (Original derivation see: Goodier JN. Appl Mech 1933:39).
[30] Dompas D, Groeninckx G. Polymer 1994;35:4743.
[31] Dompas D, Groeninckx G, Isogawa M, Hasegawa T, Kadokura M. Polymer 1994;35:4750.
[32] Dompas D, Groeninckx G, Isogawa M, Hasegawa T, Kadokura M. Polymer 1994;35:4760.
[33] Bos HL, Nusselder JH. Polymer 1994;35:2793.
[34] Kim H, Keskkula H, Paul DR. Reinforcement, impact modification and nucleation of polymers. Society of Plastic Engineers, Regional Technical Conference, Houston, 1990. 33p.
[35] Chen TK, Jan YH. Polym Engng Sci 1995;35:778.
[36] Gutek BI, vanWert B. Ind Engng Chem Prod Res Dev 1982;21:601.
[37] Bhute RS, Aggarwal JS. J Sci Ind Res 1968;27:181.
[38] Suzuki T. Netsu Kiokasei Jushi 1994;15:9.
[39] Chen TK, Jan YH. Polym Engng Sci 1995;35:778.
[40] Huo C. Tu Liao kung Yeh 1986;3:19.
[41] Kato Y. Shikizai Kyiokai Shi 1988;61:699.
[42] Ando N. Kiogyio Zairyio 1996;44:90.
[43] Akashi M. Kaobunshi Kakao 1996;45:124.
[44] Chida K, Sakaguchi S, Wagatsuma M, Kimura T. Electron Lett 1982;18:713.
[45] Shibata S, Kimura T, Sakaguchi S, Ohmori Y. Electron Lett 1984;20:662.
[46] Bogatyrjov VA, Bubnov MM. Electron Lett 1986;22:1013.
[47] Gutek BI, vanWert B. Ind Engng Chem Prod Res Dev 1982;21:601.
[48] Chen PY. Kung Yeh Chi Shu 1978;54:30.
[49] Sato A, Ushigome M, Matsumura F. IEEE 1985:9.
[50] Collins WR, Powell DB. IEEE 1985:14.
[51] Trego BR. European hybrid Microelectronics Conference, Ghent, 1979. 499p.
[52] Narula D, Be A, Yamada H. In: Proceedings of the Twenty-First Waterborne, Higher-Solids, and Powder Coatings Symposium, New Orleans, 1994. 114p.
[53] Wanf CY, Zhang JZ, Shen ZX. In: Proceedings Fifth International DUMIC, Santa Clara, CA, 1999. p. 305–11.
[54] Ban H, Tanaka A, Kawai Y, Imamura S. Polymer 1990;31:564.
[55] Zhu B, Katsoulis DE, Keryk JR, McGarry FJ. Polym Mater Sci Engng 1998;79:192.
[56] Choi SR, Salem JA. J Mater Res 1993;8:3210.
[57] ASTM Standard D 790-92.
[58] Williams JG. Fracture mechanics of polymers. New York: Ellis Horwood, 1984.
[59] Anderson TL. Fracture mechanics, fundamentals and applications. Ann Arbor: RC Press, 1995.
[60] Williams JG. Stress analysis of polymers. 2nd ed.. New York: Ellis Horwood, 1980.
[61] ASTM Standard D5045-91a.
[62] Smith AL. Spectrochim Acta 1960;16:87.
[63] Smith AL. Spectrochim Acta 1963;19:849.
[64] Smith AL, editor. The analytical chemistry of silicones New York: Wiley, 1991 (chap. 11).
[65] Durig JR, editor. Chemical, biological and industrial applications of infrared spectroscopy New York: Wiley, 1985. p. 73–85.
[66] Aldrich Library of FT-IR.
[67] Akiff JW. NMR and chemistry: an introduction to the Fourier transformation-multinuclear era. 2nd ed.. New York: Chapman and Hall, 1983.
[68] Williams EA, Cargioli JD. Annu Rep NMR Spectrosc 1979;9:221.
[69] Williams EA. Annu Rep NMR Spectrosc 1983;15:235.

[70] Williams EA, Donahue PE, Cargioli JD. Macromolecules 1981;14:1016.
[71] Williams EA, Cargioli JD, Hobbs SY. Macromolecules 1977;10:782.
[72] Zicmane ELI, Lukevics E. J Organomet Chem 1986;306:167.
[73] Franck J, Sponer H. J Chem Phys 1956;25:172.
[74] Brandt PJA, Subramanian R, Sormani PM, Ward TC, McGrath JE. Polym Prepr 1985;26:213.
[75] Levy GC, Cargioli JD. In: Axenrod T, Webb GA, editors. Nuclear magnetic resonance, spectroscopy of nuclei other than protons. New York: Wiley, 1974. p. 251.
[76] Flory PJ. Principles of polymer chemistry, Ithaca, NY: Cornell University Press, 1953. p. 509 (p. 549).
[77] Grassie N, Macfarlane IG. Eur Polym J 1978;14:875.
[78] Grassie N, Macfarlane IG, Francey KF. Eur Polym J 1979;15:415.
[79] Grassie N, Francey KF. Polym Degrad Stab 1980;2:53.
[80] Grassie N, Francey KF, Macfarlane IG. Polym Degrad Stab 1980;2:67.
[81] Clarson SJ, Semlyen JA. Siloxane polymers. Englewood Cliffs, NJ: Prentice-Hall, 1993 (chap. 5).
[82] Kerlins V., Phillips A. Modes of fracture, in metals handbook, Fractography. 9th ed., vol. 12. Metals Park, OH: American Society for Metals, 1989.
[83] Preston FW. J Am Ceram Soc 1931;14:419.
[84] Anderson TL. Fracture mechanics: fundamentals and applications. 2nd ed.. Ann Arbor: CRC press, 1995 (p. 74, 77 and 326).